ISSN 0554-6397
Izvorni znanstveni članak
(*Original scientific paper*)

Šimun Sviličić
E-mail: ssvilicic@fsb.hr
Smiljko Rudan
E-mail: smiljko.rudan@fsb.hr
Faculty of Mechanical Engineering and Naval Architecture, University of Zagreb, Ivana Lučića 5, Zagreb, Croatia

Assessing the Compression Fatigue of the Welded Test Specimens

Abstract

The focus of this paper is on compression fatigue life in welded test specimen. Considered test specimen is highly complex due to multi-layer welding and production errors affecting its topology. Test specimen is made from S355 steel which is used for both base material and weld. Compression fatigue analysis is seldom performed as compression positively affects fatigue life. At the same time, during MAG welding residual stresses affect the fatigue life, decreasing it significantly. Finite element method (FEM) is applied to estimate compression fatigue life of the welded test specimen and obtained fatigue curve is compared to the experimental curve. Experimental curves are given for different stress ratios: R= -1, and R= -∞. Analysis consists of thermal and structural analysis using FEM method and fatigue analysis which is based on FEM results. FEM thermal simulation of welding with constant initial temperature is performed first and followed by nonlinear structural analysis for assessment of the residual stresses due to heat expansion. Fatigue parameters are determined using Universal slope method.

Keywords: compression fatigue, R ratio, MAG welding, residual stress, coupled thermal-mechanic, S355

1. Introduction

Extensive research is done for the analysis of tensile fatigue. At the same time, compression and its effects are usually not considered due to its beneficial influence on fatigue life. General rule is that compression closes crack, opposed to tension which opens it [1]. This is true for cases when only compression exist but in other cases, such as in welding, this statement is not valid. Here, physical effects exist that cause residual stress such as phase transformation and distortion of crystal surfaces due to

material melting. During welding, weld is contracting in all directions: longitudinally, transversely and through thickness. Longitudinal stress causes weld distortion inwards which consequently causes tensile transversal stress in the middle of the weld [2]. This effect can be seen in Figure 1.

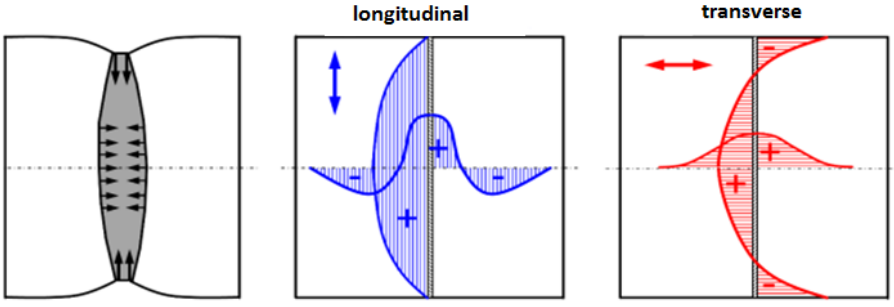

Figure 1. Weld stress [3]

Phase material transformation, volume of material, boundary conditions and geometry shape are critical variables which define residual stress. Influence of compressive, tensile, and residual stress is shown in Figure 2.

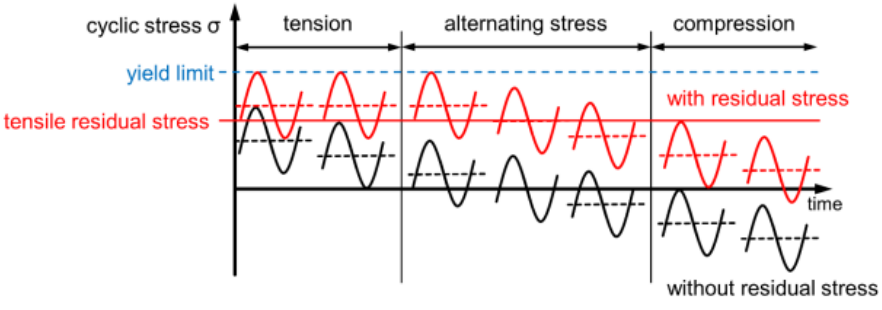

Figure 2. Influence of stress character on fatigue life [3]

Fatigue life is important parameter in designing a product, but it is hard to calculate it in real life due to many factors that influence it. Also, experimental tests are expensive, require a lot of time and resources so experimental data is often lacking. In order to investigate it more, Hamburg University of Technology conducted experiments on welded specimen submitted to alternating and compressive stress cycles, R= -1, and -∞ [4]. Test specimens were extracted from two different plates with different thickness, 25mm and 10mm respectively, with length of 250mm (both) and the width of 55mm. Dimensions of the test specimen are shown in Figure 3. During welding, U-profiles are welded on the sides so that additional deflection should not occur.

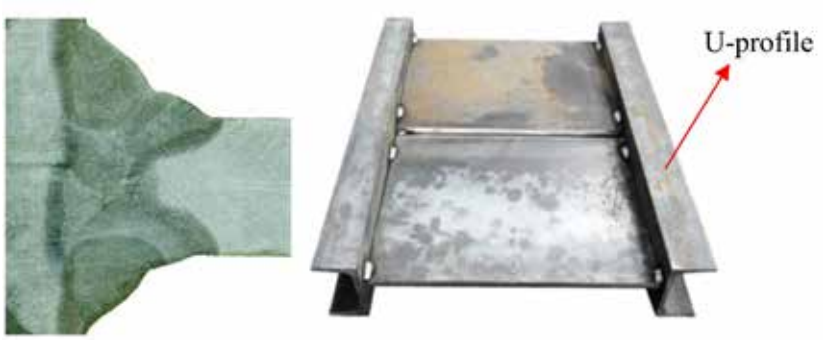

a) Test specimen *b) Set-up*

c) Dimensions

Figure 3. Test specimen [4]

Also, process of welding was monitored, and temperature measurements were done, Figure 4 [4].

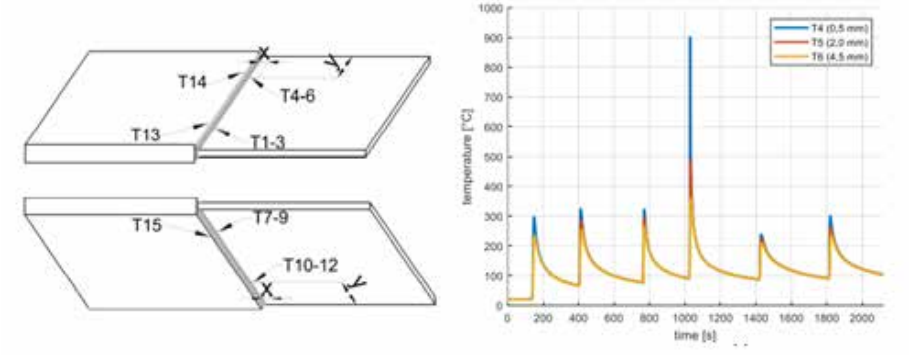

Figure 4. Thermal measurements [4]

Due to residual stress, test specimen is deformed and additional plates are introduced to minimize secondary bending during tensile test, Figure 5.

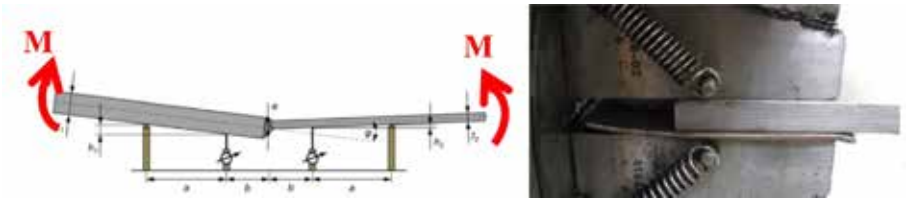

Figure 5. Test specimen deformation [4]

Residual stress is measured by two experimental methods: X-ray method and hole drilling method [3]. Hole drilling method is the most popular method for assessing residual stress [5]. Method has high variety of uses, such as in the analysis of tubular steel joints [6], or by combining it with digital image correlation for fatigue calculation [7]. For non-destructive test, X-ray method is the most popular, but accuracy is only valid up to several microns of depth [8].

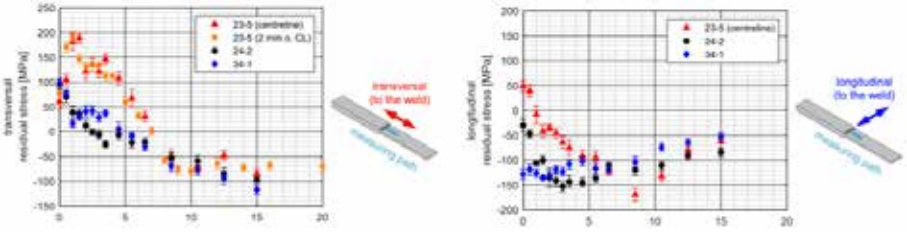

Figure 6. Residual stress [3]

There are numerous physical processes occurring during the welding (phase transformation, high thermal loads), so material properties can vary [9]. Due to uncertainty in material data properties, well known steel S355 was used [10] and metal active gas welding was chosen as a manufacturing process. Both plates and weld are made from the same already mentioned material. Fatigue calculations are commonly focused on the high cycle's fatigue, between 10^5 and 10^7 cycles while load amplitudes are constant. In the case of low cycle fatigue, calculations are based on the accurate plastic strain value which presume very accurate elastoplastic model [11]. In this work, elastoplastic model is not calibrated and tested so low cycle fatigue will not be in focus of research. Opposed to the low cycle fatigue, very high cycle fatigue with number of cycles $>10^7$ is not driven by the strain but instead by the stress. In the high cycle regime, additional factors such as surfaces treatment [12], surface integrity [13], inclusion size [14] and others are influencing the results. Even though these factors make more influence in the area of very high cycle fatigue ($>10^7$), they can start to influence around 10^6 cycle area, but this will not be covered in this article.

Goals of this research are:

- determine residual stress of the welded specimens due to high temperature and thermal expansion,
- compare residual stress values to measured values in [3],
- study influence of residual stress on the full compressive load and fatigue life in fully compressive load, R= -∞,
- compare fatigue curve obtained by numerical simulation with experimental one.

Results obtained by numerical calculation with FEM method will be compared to the experimental results done on Hamburg University of Technology [4].

2. Methodology

A methodology for fatigue life estimation based on FEM analysis using multiple ABAQUS solvers will be presented. Starting reference is the experimental test published in doctoral thesis [3] and results published by Maarstruct report [4]. Full simulation schematic is shown in Figure 7. Procedure is next:

1. First step is heat transfer analysis which consists of 12 steps: 6 steps for weld passes and 6 cooling steps in between each weld pass. Result of this analysis are nodal temperatures on the test specimen.
2. Second step is welding structural analysis: thermal expansion where nodal temperatures from previous step are applied to the identical structural mesh. Here, stress during welding is calculated due to thermal expansion.
3. A third step, structural analysis: tensile test is test where test specimen is subjected to tensile load with residual stress incorporated from previous step.
4. Last step is the fatigue analysis where stress field is transferred from structural analysis: tensile test to fatigue calculation software, FE-SAFE. Here, number of cycles until failure are calculated for every nominal load applied.

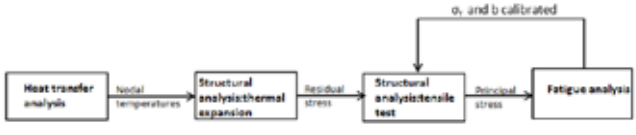

Figure 7. Schematic of simulation method

Despite the advanced approach presented, many variables could affect the accuracy of the results. Some of them are: material property data, manufacturing process deviations, symmetry condition, inadequate fatigue parameters etc. So initially, Basquin equation parameters are calibrated for R= -1 with less than 5% correction. Referent curve and corresponding loads are shown in Figure 8. After this, tensile test is done for full compression, R= -∞ by using fatigue parameters previously calibrated for R= -1.

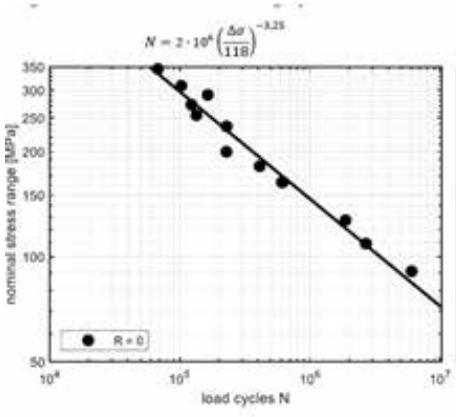

Fmin [kN]	Fmax [kN]	Nominal stress range [MPa]	Load cycles N
0	160	290,91	163830
0	150	272,73	122683
0	170	309,09	102600
0	190	345,45	67796
0	130	236,36	228488
0	110	200,00	227921
0	70	127,27	1874139
0	50	90,91	6023907
0	90	163,64	607880
0	60	109,09	2682988
0	140	254,55	134052
0	90	163,64	617751
0	100	181,82	409970

Figure 8. Reference experimental curve [4]

2.1. Heat transfer analysis

Heat transfer analysis solves heat generation problem in solids under thermal load. This solver can solve both steady state and transient cases. In welding simulation, only transient case should be considered due to variable heat input. Nonlinearities in this type of analysis comes from either nonlinear boundary conditions or from material properties that are temperature dependent. Nonlinearity from material properties is usually mild because properties do not change rapidly with the temperature. Formula for heat transfer analysis can be written through energy balance equation:

$$\int_V \rho \dot{U}\, dV = \int_S q dS + \int_V r\, dV \tag{1}$$

where V is a volume of solid material, S surface area, ρ is the density of the material, $\dot{U}$ is the material time rate of the internal energy, q is the heat flux per unit area of the body and r is the external heat source. Here, it is assumed that analysis is uncoupled in the sense that temperature of the material does not depend on strains and displacements of the body. Heat is inputted in the analysis through constant temperature method using "death and birth element" method. This means that analysis is introducing elements at a constant temperature which is equivalent to the melting temperature. In order to solve this, diffusive elements are used which allows heat storage and heat conduction. These elements only have temperature degrees of freedom. Output results are the nodal temperature. To define heat transfer analysis, data on conduction, convection, and thermal capacity should be provided [10].

2.2. Structural analysis

Structural analysis solves equation:

$$[K_T]\{\Delta u\} = \{F\} - \{F^{nr}\}, \tag{2}$$

where $[K_T]$ is tangent stiffness matrix, $\{\Delta u\}$ is displacement increment, is external load and $\{F^{nr}\}$ is internal force vector. Solver iteratively solves this equation based on Newton – Raphson method by gradually increasing load at each increment and calculates equilibrium equations. When equilibrium iteration is within specified tolerance, solver is continuing to the next increment. Maximum size of the increment is defined by the load amplitude input, in this case temperature. Incremental plasticity theory with isotropic hardening is used which defines post-yield behavior by defining true stress-strain diagram after yield. Plastic curves and thermal expansion coefficients are defined for this problem as temperature dependent [10].

2.3. Fatigue calculation

There are multiple ways and equations how to calculate fatigue and usage of them is based on assumptions, material, and recommendations. Here, calculations are based on the Basquin equation [15]. Since stress ratio is different than -1, mean stress effect exists. Brown Miller algorithm was used following the recommendations [16].

$$\sigma_A = \sigma_f^{'} N^b, \tag{3}$$

where σ_A is stress amplitude, N number of cycles, σ'_f and b are Basquin parameters. Output parameter is number of cycles until failure.

3. Results

Due to limited computational resources, total simulation time is reduced with factor of 2 by increasing air convection coefficient from standard 10 W/m^{2}K to 40 W/m^{2}K. Other parameters for heat transfer analysis are: conduction set to 45 W/m^{2}K and specific heat set up to 455 J/kg K at a room temperature. Width of test specimen, Figure 9, is reduced with the usage of symmetry boundary condition from 55mm to 27.5mm. Elements that are used for heat transfer analysis are second order hexahedral DC3D20 with average element size in each direction is 8mm and critical weld areas are locally refined. The melting temperature of the weld is 1450 ^{o}C. Focus during the meshing is on the weld and the critical area which is transition from the weld to the thinner plate.

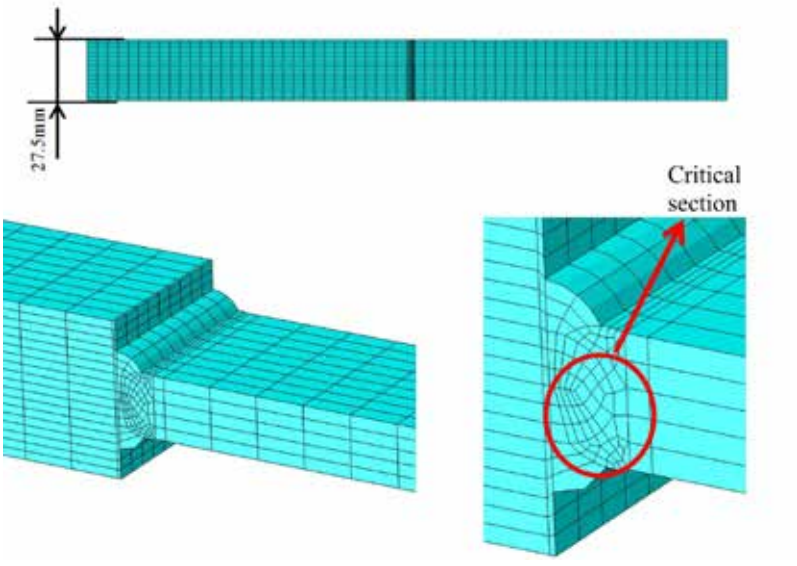

Figure 9. Test specimen dimensions and mesh (zoom on the right)

In Figure 10, temperature distribution is compared between actual measurement on the Hamburg University of Technology [4] and simulation measurement. Results are given for the same points, shown in Figure 4. Three points are measured on different locations: 0.5mm, 2.5mm and 5mm from the weld. Correlation of the results is excellent between measurement and reduced heat transfer simulation. With this, it can be said that increasing air convection coefficient α is justified.

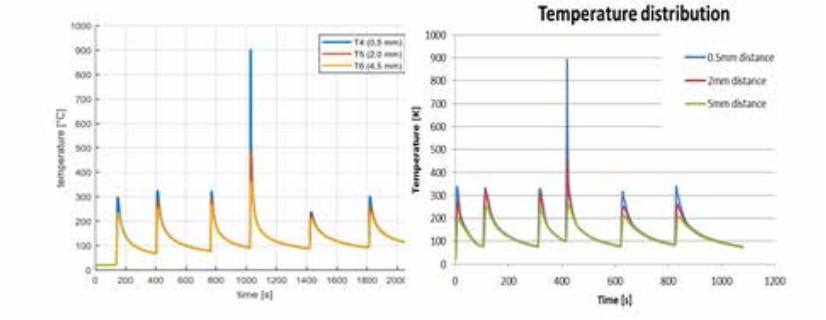

a) *b)*

Figure 10. Thermal distribution: a) measurement [4], b) simulation

Temperature results are applied on the compatible structural mesh. Boundary conditions are shown in Figure 11. For the heat transfer analysis, only symmetry boundary conditions are applied. For the structural analysis: thermal expansion, two additional nodes are constrained as shown in Figure 11 a). Reason why they are fixed is that in actual welding, additional U-profiles are spot welded on the side to prevent rotation and displacement of the plate in these sides (Figure 5). Without those additional boundaries, test specimen would freely rotate. For tensile test, only symmetry and fixation on the surface is used. Linear expansion coefficient is equal to 1.2

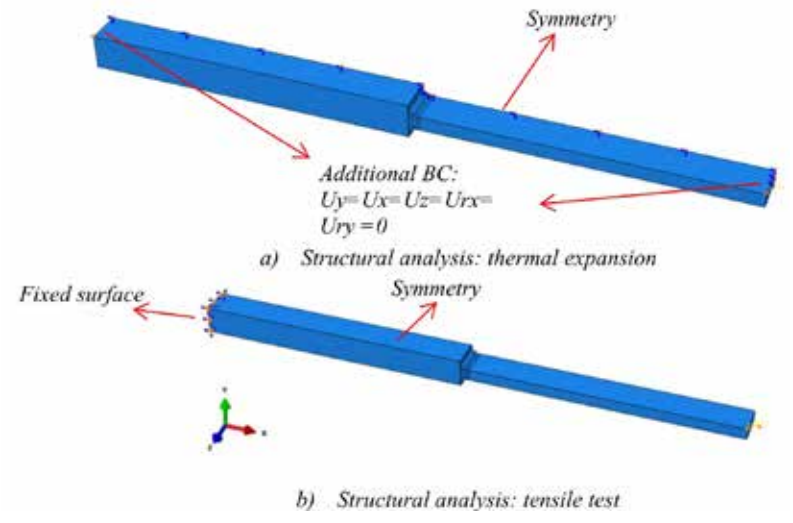

Figure 11. Boundary conditions

Simulation showed model angular deformation is similar to the test specimen angular deformation after welding (Figure 12). Test specimen is bending due to the thermal expansion [4].

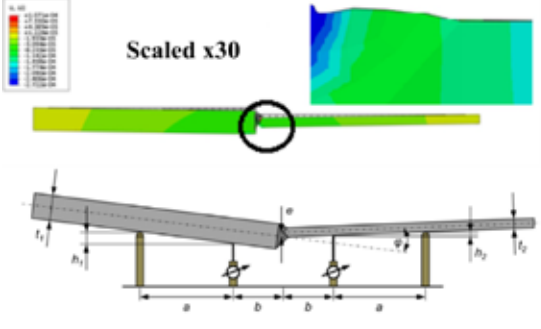

	Angular deformation [°]
Experiment	0.33
Simulation	0.304

Figure 12. Deformation after welding

Progression of plastic deformation during time is presented in Figure 13. Plastic deformation is occurring in different zones at a different time depending on the welding progress. This is causing asymmetrical plastic deformation and residual stress. It can be seen on Figure 13 that area with elements where Weld pass 1 is applied has much higher plastic strain than on the last Weld pass 6. Reason why is that even though largest percentage of plastic strain is caused during phase transformation and melting, neighboring welds are influencing development of plastic strain which is rising. Weld 1 does not experience only phase transformation during welding but also temperature increase during surrounding weld passes. On the other hand, Weld pass 6 is the last welding pass so it will only experience phase transformation.

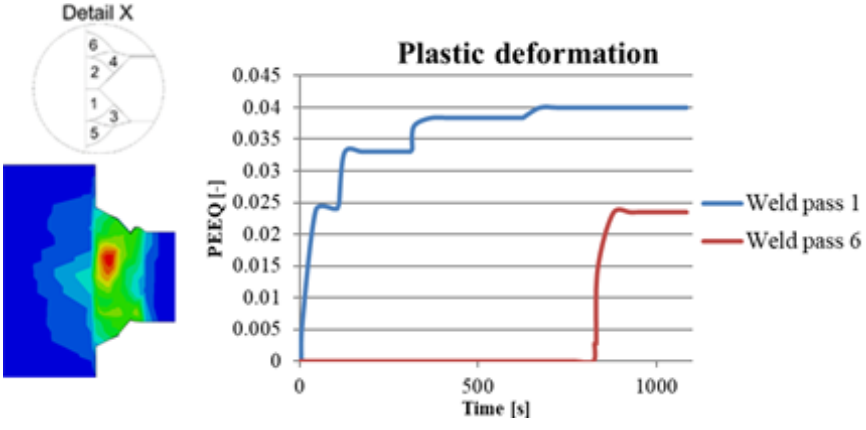

Figure 13. Plastic deformation zones

Longitudinal stress is shown in Figure 14 and it is compared with the measurement from [3]: both hole drilling and X-ray methods are compared with the simulation.

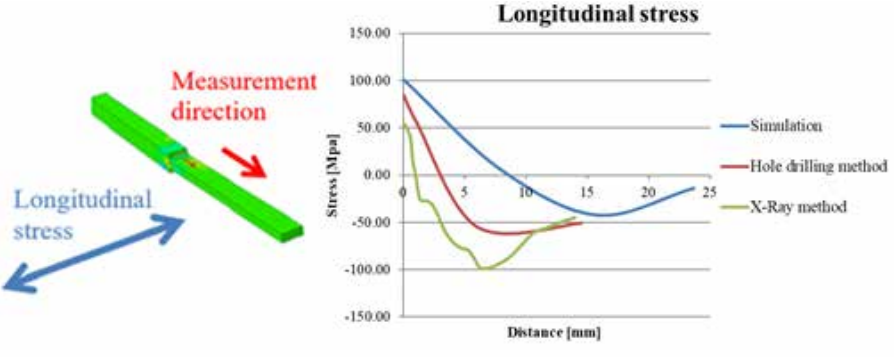

Figure 14. Longitudinal stress

Simulation differs from both measurement methods at the proximity of the weld and the gap is smaller away from the weld. Longitudinal stress is not critical in this case because it will not superimpose with the stress from tensile test.

Transverse stress is the most important as it has the same direction as the stress caused by the tension that will be applied afterwards. It can be seen in Figure 15 that results in proximity to the weld are extremely close, <2% difference, which is important because this is the location of critical section. Away from the weld, stress results differ which could be result of using the same material properties for heat affected zone and the rest of the specimen.

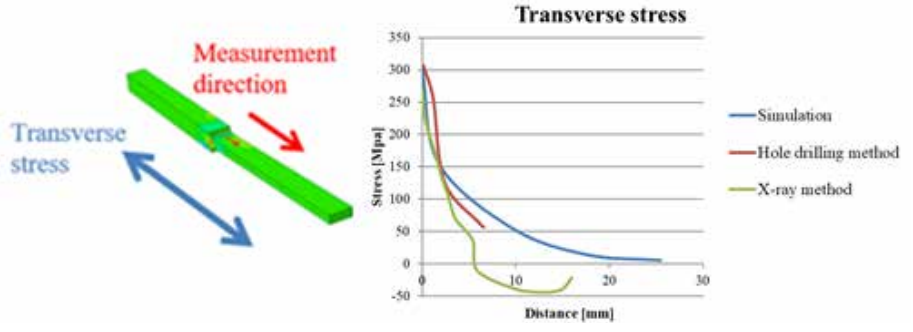

Figure 15. Transverse stress

Results given by FEM method are applied in the numerical software FE-SAFE for fatigue calculation. Fatigue life curve and corresponding cycles are calculated with the Basquin equation while Brown Miller algorithm is used for the mean stress correction. Plastic deformations are not used in fatigue calculation because they occurred only during welding and force used in tensile test is too low to cause further plastic strain increase. This means that plastic strain will not cycle but instead will have a constant value.

Values for fatigue parameters are initially calculated by Universal slope method (modified by Mason and Muarlidharan [17]).

$$\sigma_f^{'} = E \cdot 0.623 \left(\frac{\sigma_m}{E} \right)^{0.832} \tag{4}$$

$$b = -0.09 \tag{5}$$

where $\sigma'_f = 885$ and b= -0.09 are results from (4) and (5). Angular deformation is captured with FEM while linear misalignment will be applied as factor:

$$k_{m,e} = 1 + 3\frac{e}{t} = 1.033 \tag{6}$$

Linear misalignment is hard to physically model for small deformations, less than 1mm [18] but instead, it is usually implemented as a factor [19]. Also, it is shown that this is acceptable [20].

Initial results are calculated for the stress ratio of R= -1 and compared to the referent curve, Figure 8. Fatigue life calculations estimates 290000 cycles until failure for a nominal stress of 200 MPa. With this, small calibration of the Basquin parameters calculated by Universal slope method should be done. Only σ'_f is calibrated by a little margin, from 885 to 878. Second parameter, b which defines fatigue life curve slope was not calibrated.

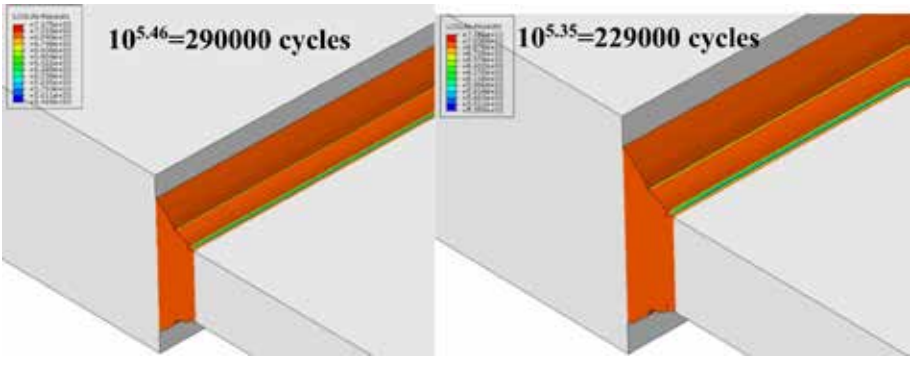

a) σ'_f *=885* *b)* σ'_f *=878*

Figure 16. Fatigue life calibration for R=-1: a) calculated σ'_f *and b) calibrated* σ'_f

Finally, results comparison for the full compression, R= -∞ are shown in Figure 17. It can be noticed that in lower area of fatigue, $<10^6$ cycles, results are close enough with the difference of 10%, but when going into area above 2 million cycles, results diverge significantly, >100%. Reason for this cannot be known without additional test of material properties and their dependency on temperature, surface treatment factors (having an increasing influence at higher number of cycles), etc. This is out of the scope of this article and could be done in future research.

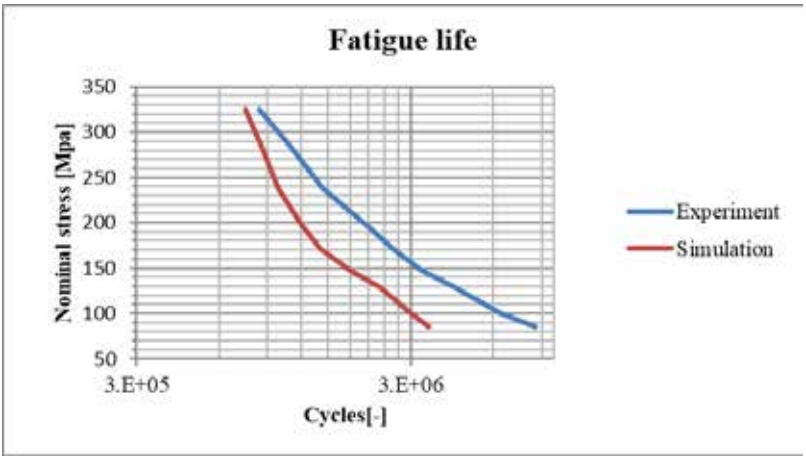

Figure 17. Comparison of the results for R= - ∞

4. Discussion

Deviation from experimental testing can occur from many different reasons. One of them is lack of fatigue data and repeatability of the test specimen testing. Second reason is control of manufacturing and geometrical sensitivity of the test specimen. Additional parametric study was done to test the sensitivity of results on the weld geometry. High discrepancy between maximum stresses in the case of local weld radius change was noticed. In the parametric study, nominal force of 160 kN was applied as a tensile force and two radii are changed: between Weld pass 4 and Weld pass 6 and between thinner plate and Weld pass 6. It can be seen that for a small change of radius, 0.0035 to 0.0045mm, stress can increase from 450 to 541 MPa which is over 20%.

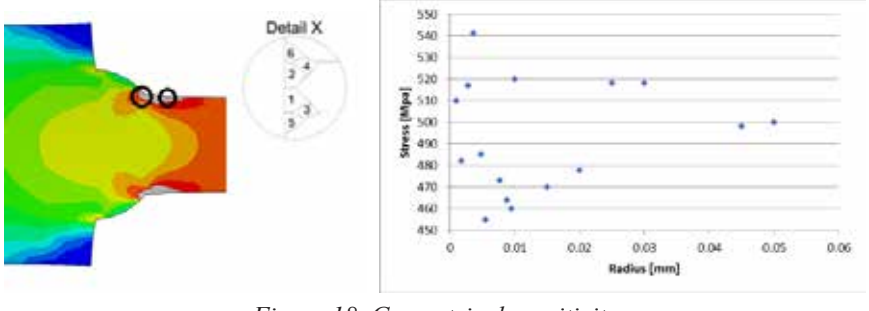

Figure 18. Geometrical sensitivity

Factors of surface treatment are not included in the analysis which can also lead to the wrong results in the higher fatigue area.

5. Conclusions

Compression fatigue calculation is presented in the paper.

Heat transfer analysis using constant temperature reached satisfactory results. Temperature measurement in experiment and simulation differ by less than 5% so it can be concluded that chosen material model with time reduction captures heat transfer behaviour correctly leading to correct analysis.

Structural analysis: thermal expansion, showed different results than those measured. Longitudinal stress showed rather high deviation from measurement, but transversal stress showed good fit close to the weld root. Away from the weld, results differ. It is suspected that heat affected zone is not adequately modelled or elastoplastic material model is not adequate. Further research should focus on modelling heat affected zone with different material properties and investigate elastoplastic model and its dependency on temperature.

Even with rather inaccurate longitudinal residual stress, fatigue analysis showed satisfactory results for less than 1 million cycles. Difference between simulation and experiment was in the range between 10 and 20 %. This is because transverse stress is more important, and it was much closer to the measurements. Higher number of cycles diverged from the testing with giving only half of number of cycles that experiment gave. This could be due to numerous reasons: beneficiary behaviour of multiple factors such as surface treatment on the fatigue life or limitation in fatigue algorithms for the analysis. Additionally, slope of the fatigue life curve which depends on the Basquin parameter *b* should be further calibrated.

Nomenclature

Abbreviations:

MAG	Metal active gas
FEM	Finite element method
SN	Stress-Number of cycles

Latin Symbols:

b	Basquin exponent (-)
$k_{m_{,e}}$	linear misalignment factor (-)
N	number of cycles (-)

Greek symbols:

α	convection transfer coefficient (W/m^{2}K)
σ	stress (MPa)
σ'_f	Basquin parameter (MPa)
σ_m	mean stress (MPa)

Subscripts:

x longitudinal direction
y transverse direction
z thickness direction

6. References

1. Lietaert, K., Cutolo, A., Boey, D. & Van Hooreweder, B. (2018) Fatigue life of additively manufactured Ti6Al4V scaffolds under tension-tension, tension-compression and compression-compression fatigue load. *Scientific Reports.* 8, 4957. Available at: https://doi.org/10.1038/s41598-018-23414-2 [Accessed on 16. March. 2021].
2. Dev, A. & Saha, M. (2017) Ship Repairing Time and Labour. *MARTECH 2017; 12th Biennial International Conference and Exhibition Towards 2030: Maritime Sustainability through People and Technology.* Available at: https://ssrn.com/abstract=3753689 [Accessed on 16. March. 2021].
3. Friedrich, N. (2021) *Approach to consider welding residual stresses in fatigue analysis using numerical simulations*. Ph. D. Technischen Universität Hamburg.
4. Freidrich, N. & Ehlers, S. (2018) Fatigue life prediction of welds for different stress ratios R. *Marstruct*. Available at: http://www.marstruct-vi.com/marstruct2021/structure.aspx [Accessed on 3. March 2020].
5. Schajer, G. S. & Whitehead, P. S. (2018) *Hole-Drilling Method for Measuring Residual Stresses*. Synthesis SEM Lectures on Experimental Mechanics. Available at: https://doi.org/10.2200/S00818ED1V01Y201712SEM001 [Accessed on 20. March. 2021].
6. Van Puymbroeck, E., Nagy, W., Fang, H. & De Backer, H. (2018) Determination of residual weld stresses with the incremental hole-drilling method in tubular steel bridge joints. *Procedia Engineering.* 213, 651-661. Available at: https://doi.org/10.1016/j.proeng.2018.02.061 [Accessed on 21. March 2021].
7. Peng, Y., Zhao, J., Chen, L. & Dong, J. (2021) Residual stress measurement combining blind-hole drilling and digital image correlation approach. *Journal of Construction Steel Research*. 176, 106346. Available at: https://doi.org/10.1016/j.jcsr.2020.106346 [Accessed on 21. March 2021].
8. Lai, H. & Wu. W. (2020) Practical examination of the welding residual stress in view of low-carbon steel welds. *Journal of Materials Research and Technology*. 9(3), 2717-2726. Available at: https://doi.org/10.1016/j.jmrt.2020.01.004 [Accessed on 21. March 2021].
9. Winczek, J., Gawronska, E., Gucwa, M. & Sczygiol, N. (2019) Theoretical and Experimental Investigation of Temperature and Phase Transformation during SAW Overlaying. *Applied Science*. 9(7), 1472. Available at: https://doi.org/10.3390/app9071472 [Accessed on 23. March 2021].
10. Piekarska, W., Saternus, Z., Sapieta, M. & Kopas, P. (2020) Numerical and experimental analysis of a laser welded joint made of dissimilar materials S355 and 304 steel. *IOP Conference Series Materials Science and Engineering*. 776(1), 012075. Available at: https://iopscience.iop.org/article/10.1088/1757-899X/776/1/012075 [Accessed at 25. March 2021].
11. Zhang, J., Li, W., Dai, H., Liu, N. & Lin, J. (2020) Study on the Elastic–Plastic Correlation of Low-Cycle Fatigue for Variable Asymmetric Loadings. *Materials*. 13(11), 2451. Available at: https://doi.org/10.3390/ma13112451 [Accessed on 27. March 2021].
12. Song, Z., Gao, W., Wang, D., Wu, Z., Yan, M., Huang, L. & Zhang, X. (2021) Very-High-Cycle Fatigue Behavior of Inconel 718 Alloy Fabricated by Selective Laser Melting at Elevated Temperature. *Metals*. 14(4), 1001. Available at: https://doi.org/10.3390/ma14041001 [Accessed on 1. April 2021].
13. Fu, H. & Liang, Y. (2021) Study of the Surface Integrity and High Cycle Fatigue Performance of AISI 4340 Steel after Composite Surface Modification. *Metals*. 9(8), 856. Available at: https://doi.org/10.3390/met9080856 [Accessed on 2. April 2021].
14. Li, S. X. (2013) Effects of inclusions on very high cycle fatigue properties of high strength steels. *International Materials Reviews*. 57(12). 92-114. Available at: https://doi.org/10.1179/1743280411Y.0000000008 [Accessed on 2. April 2021].
15. Wen, X., Wang, P., Dong, Z., Liu, Y. & Fang, H. (2018) Nominal Stress-Based Equal-Fatigue-

Bearing-Capacity Design of under-matched HSLA Steel Butt-welded Joints. *Metals*. 8(11), 880. Available at: https://doi.org/10.3390/met8110880 [Accessed on 4. April 2021].
16. Barraza, J., Monarrez, M. R. & Molina, R. (2020) Fatigue-Life Prediction of Mechanical Element by Using the Weibull Distribution. *Applied Science*. 10(18), 6384. Available at: https://doi.org/10.3390/app10186384 [Accessed on 5. April 2021].
17. Muralidharan, U. & Manson, S.S. (1988) A Modified Universal Slopes Equation for Estimation of Fatigue Characteristics of Metals. *Journal of Engineering Materials and Technology*. 110(1), 55-84. Available at https://doi.org/10.1115/1.3226010 [Accessed on 5. April 2021].
18. Ottersböck, M.J., Leitner, M., Stoschka, M. & Maurer W. (2019) Analysis of fatigue notch effect due to axial misalignment for ultrahigh-strength steel butt joints. *Welding in the World*. 63(1). 851-865. Available at: https://doi.org/10.1007/s40194-019-00713-4 [Accessed on 7. April 2021].
19. Xing, S. & Dong, P. (2016) An analytical SCF solution method for joint misalignments and application in fatigue test data interpretation. *Marine structures*. 50(1). 143-161. Available from: https://doi.org/10.1016/j.marstruc.2016.07.006 [Accessed on 7. April 2021].
20. Taras, H. & Unterweger, H. (2017) Numerical Methods for the fatigue assessment of welded joints: Influence of misalignment and geometric weld imperfections. *Engineering Structures*. 9(1). 9-24. Available at: https://doi.org/10.3846/2029882X.2017.1299968 [Accessed on 7. April 2021].
21. Niesłony, A. & Böhm, M. (2013) Mean stress effect correction using constant stress ratio S–N curves. *International Journal of Fatigue*. 52. 49-56, Available at: https://doi.org/10.1016/j.ijfatigue.2013.02.019 [Accessed on 9. April 2021].

7. APPENDIX

Opposed to the complex study shown in the article, two other approaches were tried in order to see can the compressive fatigue be solved with less complex methods and possibly save significant amount of time.

7.1 Analytical approach

First approach is done by linear regression [21] which takes into the account mean stress correction:

$$N = 2 \cdot 10^6 \cdot \left(\frac{\Delta\sigma}{118}\right)^{-3.25} \tag{7}$$

$$\Delta\sigma_{eg} = \frac{\sigma_a}{1-\frac{\sigma_m}{R_m}} \tag{8}$$

where $\Delta\sigma$ is equivalent stress amplitude, R_m tensile strength, σ_m mean stress and N number of cycles. Here, Morrow mean stress correction is taken.

$$\frac{N_{R\neq-1}}{N_{R=-1}} = \frac{2\cdot 10^6 \cdot \left(\frac{\sigma_{a,R\neq-1}}{118\cdot\left(1-\frac{\sigma_{m,R\neq-1}}{R_m}\right)}\right)^{-3.25}}{2\cdot 10^6 \cdot \left(\frac{\sigma_{a,R=-1}}{118}\right)^{-3.25}} => N_{R\neq-1} =$$

$$N_{R=-1}\cdot\left(\frac{\sigma_{a,R\neq-1}}{\left(1-\frac{\sigma_{m,R\neq-1}}{R_m}\right)\cdot\sigma_{a,R=-1}}\right) \quad (9)$$

With this formula, mean stress effect is taken into the account so fatigue curves can be cone for different stress ratios R=-1, -∞ or different stress amplitudes

Disadvantages of this approach is that does not include any physical effect or any residual stress nor mean stress amplitude changes value with the change of load direction (tension/compression). Results approximated for R=-∞ are shown in Figure 19.

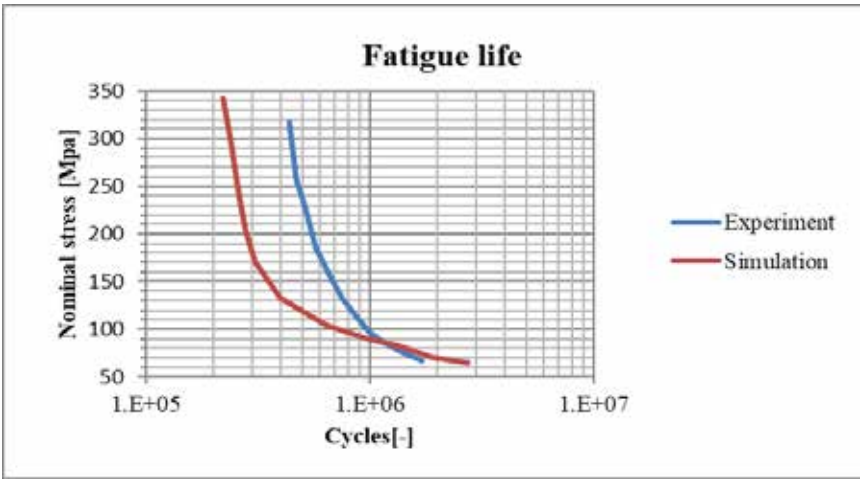

Figure 19. Fatigue curve for R=- with first approach

Results in Figure 19 show that the slope of the tested curve is completely different then the experiment and it will accurately predict only zone around 5 million cycles. Opposed to the experimental curve which has big slope due to residual tensile stress, curve gain by first approach is not showing this behaviour. This approach should not be regarded as valid.

7.2 Elastic approach

Second approach combines linear elastic FEM model by using second order hexahedral elements, C3D20 and fatigue calculation. Design of test specimen, Figure 8 is reversely engineered from the presented test specimen [4] and this will be used for calculation. Newly designed test specimen is shown in Figure 20.

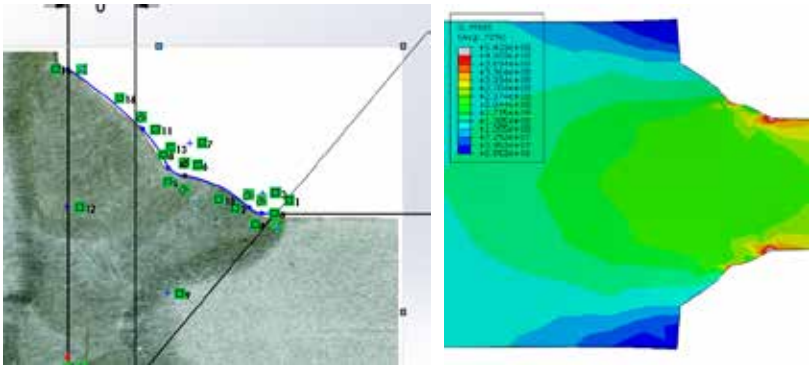

[3]

Figure 20. Reversible test specimen

Fatigue curve is first calibrated for the R= -1 curve and then it was used for R= -. For nominal stress of 200 MPa, maximum stress goes up to 400 MPa which leads to the stress concentration of 2. In order to get fatigue curve, fatigue parameters will need to be solved. For this fatigue area, Basquin equation is used so parameters that are calibrated are σ_f and b.

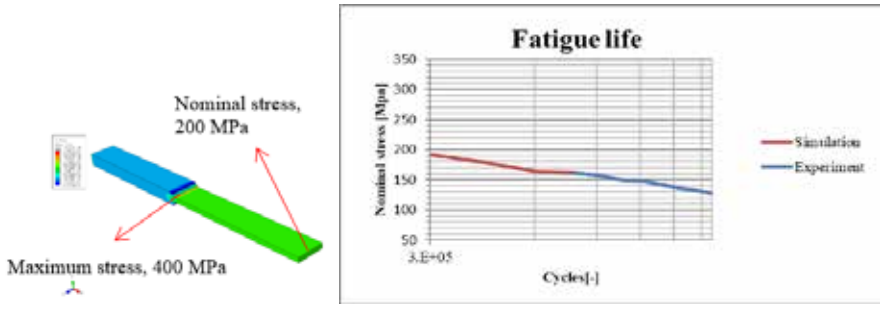

a) FEM model *b) Fatigue curves for R=-1*

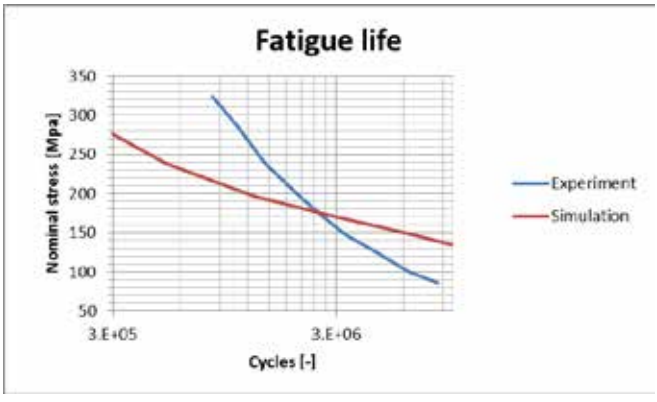

c) Fatigue curves for R= -∞

Figure 21. Second approach

Disadvantage of this approach is that no physical effect is model but instead, replaced with artificially increased value of Basquin parameters by calibrating it with reference R= -1 model. Curve shown in Figure 21 for R= -∞ is not accurately representing the fatigue live. For low cycle's fatigue, it is undervaluing the life and for higher cycles fatigue it is overvaluing the life. Again, reason behind this is that residual stress from welding is missing as a physical effect. This approach should not be regarded as valid.